CamTuner: Reinforcement-Learning based System for Camera Parameter Tuning to enhance Analytics

Sibendu Paul* Purdue University West Lafayette, USA paul90@purdue.edu

Murugan Sankaradas NEC Laboratories America New Jersey, USA murugs@nec-labs.com Kunal Rao NEC Laboratories America New Jersey, USA kunal@nec-labs.com

Oliver Po NEC Laboratories America New Jersey, USA oliver@nec-labs.com

Srimat T. Chakradhar NEC Laboratories America New Jersey, USA chak@nec-labs.com Giuseppe Coviello NEC Laboratories America New Jersey, USA giuseppe.coviello@nec-labs.com

> Y. Charlie Hu Purdue University West Lafayette, USA ychu@purdue.edu

ABSTRACT

Complex sensors like video cameras include tens of configurable parameters, which can be set by end-users to customize the sensors to specific application scenarios. Although parameter settings significantly affect the quality of the sensor output, and the accuracy of insights derived from sensor data, most end-users use a fixed parameter setting because they lack the skill or understanding to appropriately configure these parameters. We propose CamTuner, which is a system to automatically, and dynamically adapt the complex sensor to changing environmental conditions. We show that by automatically, and dynamically updating the parameter settings to adjust to the changing environmental conditions near the sensor, it is possible to significantly improve the accuracy of inferred insights. CamTuner includes two key components. First, a bespoke analytics quality estimator, which is a deep-learning model to automatically and continuously estimate the quality of insights from an analytics unit as the environmental conditions around a sensor change. Second, a reinforcement learning (RL) module, which reacts to the changes in quality (as perceived by the quality estimator), and automatically adjusts the camera parameters to enhance the accuracy of insights.

We improve the training time of the RL module by an order of magnitude by designing two virtual models to mimic the essential behavior of the camera: we design *virtual knobs* that can be set to different values to mimic the effects of assigning different values to the camera's configurable parameters, and we design a *virtual camera* model that mimics the output from a video camera at different times of the day. These virtual models significantly accelerate training because (a) frame rates from a real camera are limited to 25 to 30 fps while the virtual models enable processing rate of 300 fps, (b) we do not have to wait until the real camera sees different environmental conditions, which could take weeks or months, and (c) virtual knobs can be updated instantly, while it can take 200-500 ms to change the camera parameter settings using APIs provided by the camera-vendor. Our dynamic tuning approach results in up

to 12% improvement in the accuracy of insights from several video analytics tasks. Also, *CamTuner*'s sensor modelling and dynamic tuning methodology can be used to automatically, and dynamically tune other complex sensors.

KEYWORDS

sensor tuning, video analytics, reinforcement learning, sensor modelling, virtual camera, virtual knobs

1 INTRODUCTION

Due to the growing demand for automation and the impetus to make everything "smart", the global smart sensor market size is expected to grow from US \$36 billion in 2020 to US \$88 billion by 2025, at a CAGR of 19 % [3]. Sensors are the eyes and ears of any automation system. Some sensors like pressure or temperature transducers are simple, but as more and more features are added, the complexity of the sensors is increasing. For example, complex sensors like video cameras, thermal cameras and lidars include an increasing array of features and tens of configurable parameters, which can be set by end users to customize the sensors to specific application scenarios [51] [55]. Although values for the configurable parameters determine the quality and information content in the sensor output, and this directly impacts the quality of insights obtained from AI and machine learning models that process the sensor data streams, most end-users do not have the skill or understanding to appropriately configure these parameters. Furthermore, the environmental conditions around the sensors can vary considerably [36] during the lifetime of the sensor applications, and the values for the configurable parameters may have to be updated multiple times to ensure consistent, high quality sensor output and highly accurate insights from the sensor data.

Using a video camera (which exposes tens of configurable parameters to end-users) as a representative complex sensor, we

^{*}Work done as an intern at NEC Laboratories America.

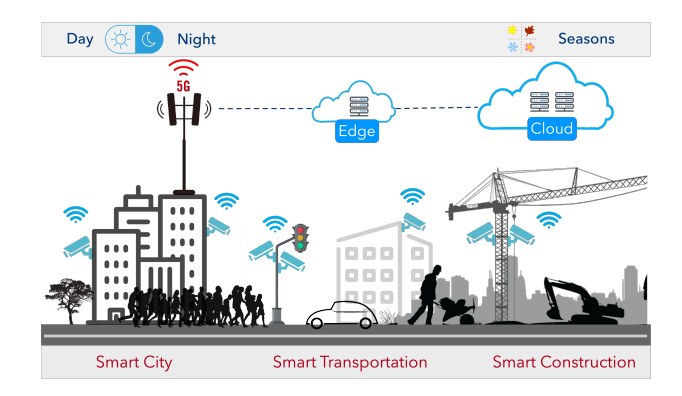


Figure 1: City-scale video analytics

propose a system, called *CamTuner*, that automatically, and dynamically adapts the complex sensor to changing environmental conditions. Such dynamic tuning improves the accuracy of insights from video analytics. Due to the significant progress in machine learning and computer vision techniques for processing video streams [25], growth in Internet of Things (IoT), edge computing and high-bandwidth communication links like 5G [9, 34], video analytics market is estimated to grow from \$5 billion in 2020 to \$21 billion by 2027, at a CAGR of 22.70 % [17]. Cameras are increasingly being deployed throughout the world in city-scale applications like surveillance, transportation, and public safety where different types of video analytics tasks are being performed on thousands of video feeds, as shown in Figure 1.

CamTuner's sensor modelling and dynamic tuning approach can also be used to automatically, and dynamically tune other complex sensors. For example, a thermal camera exposes several parameters like object emissivity, atmospheric transmission, and ambient temperature for temperature compensation. The proposed techniques can be used to dynamically tune these parameters as environmental conditions (like lighting, relative humidity, reflective surfaces and ambient temperature) change, and ensure consistent, highly accurate temperature measurements.

Depending on the video analytics task, cameras may be deployed either indoors or outdoors (Figure 1. For example, video cameras for traffic analytics are deployed outdoors (pointing towards roads or highways), whereas for contactless fever screening of passengers disembarking from an airplane, the visual and thermal cameras are deployed indoors (pointing towards the boarding gates). Furthermore, for the same video analytics task like video surveillance, cameras may be deployed indoors (in hallways inside a building) or outdoors (parking lots, for example). Clearly, different analytics tasks require different placements of video cameras and these cameras also view significantly different scenes. Also, depending on the environmental conditions, there may be natural lighting from the sun, artificial lighting or a combination of both. This can lead to bright or dark scenes and the lighting can vary over time (especially for outdoor locations) based on the weather conditions (cloudy, sunny, rainy, foggy, etc.) and time of the day (dawn, morning, afternoon, evening, dusk, twilight, night, etc.).

Lighting can also vary in indoor locations depending on the placement of cameras and the amount of artificial and natural light in that location. The particular direction of arrival of light can also change the way the scene is captured by the video camera due to projection of shadows. Different camera placements, applications and deployment conditions, as shown in Fig. 1, are just a few examples of many, dynamically changing factors that affect the accuracy of insights derived using video analytics. For real-time analytics and response, the accuracy of insights depends on the most recently observed video frames, whose quality and information content is directly impacted by the current camera parameter settings and ambient conditions near the camera. In this paper, we refer to a specific video analytics task as an *analytics unit* or AU.

Recognizing that a single, fixed setting of camera parameter values is inadequate to ensure consistent, high quality sensor output when environmental conditions change, we propose CamTuner. It is an automatic and dynamic system that adjusts to changing environmental conditions by suitably modifying the values of the configurable camera parameters. The modified settings result in higher quality sensor output, which in turn results in more accurate insights from machine learning models that process the sensor data. CamTuner includes two important components. First, an analytics quality estimator, which is a deep-learning model to automatically estimate the quality of insights from an analytics unit. As the environmental conditions around a sensor change, any change in accuracy of insights from the analytics unit is automatically detected by the AU-specific analytics quality estimator. Since different quality evaluation methods are typically used to estimate the quality of insights from different analytics units (this is described in Section 4.1), our quality estimator is AU-specific. However, our approach to design the quality estimator can be used to derive different AU-specific estimators (we present AU-specific analytics quality estimators for three different types of analytics units). Second, a Reinforcement Learning (RL) module, which reacts to the changes in quality, as perceived by the quality estimator, and automatically adjust the camera parameters to enhance the quality of insights (described in Section 4.2).

Training the reinforcement learner from scratch by using a real camera setup can be time-consuming because (a) we have to wait until the real camera observes different environmental conditions (b) we can process the frames only at the speed at which they are produced by the real camera e.g. 25 to 30 FPS and (c) for every action taken by the RL agent, depending on the camera, it can take 200-500 ms to change the camera parameter settings using APIs provided by the camera-vendor. To reduce the training time by an order of magnitude, we propose two virtual models to mimic the essential behavior of the camera: we design virtual knobs that can be set to different values to mimic the effects of assigning different values to the camera's configurable parameters, and we design a virtual camera model that mimics the output from a video camera at different times of the day. The virtual knobs model (described in Section 3.1) allows the application of different camera parameter settings to the same input scene (something that is not possible to do with the real camera because only one set of camera parameter values can be in effect at any given time).

The virtual camera model (described in Section 5) allows rerendering of any video sequence for different environmental conditions. This is especially useful to quickly train the reinforcement learning model because multiple versions of a video sequence with

known ground truth can be quickly rendered for different environmental conditions. Again, such a re-rendering of the same video scene for different environmental conditions is not possible with a real camera. Besides, with the help of virtual camera, we can process frames at a much faster rate, even upto 300 FPS by using more computing hardware. Using the virtual camera model, days worth of videos can be processed within hours. Also, for the RL agent, each action can be performed within 10s of milliseconds by using virtual knobs, which otherwise would take hundreds of milliseconds with real cameras. By combining these characteristics of the virtual models, where (a) we can render various environmental conditions (b) process frames at much higher speed and (c) take actions very quickly, we can train the RL module significantly faster (greater than 10x speedup).

We train the proposed reinforcement learning module using a system consisting of the virtual camera, virtual knobs, the analytics unit, and its quality estimator. After such training, the reinforcement model is deployed and continuously fine-tuned in the real deployment by using video data from the real camera. *CamTuner* can be used to automatically create and fine-tune reinforcement learning models for thousands of cameras in large-scale deployments like city-wide surveillance systems.

In this paper, we make the following contributions:

- (1) We empirically show that a fixed set of values for the camera parameters does not lead to consistent, high-quality insights as environmental conditions change. Rather, the desirable camera setting varies as environmental conditions change. Also, the desired camera parameter setting varies across different analytics units for the same environmental conditions. This motivates the need for automatic and dynamic adjustment of camera parameters as analytics tasks and environmental conditions change.
- (2) We propose a new methodology to design *AU-specific An*alytics Quality Estimator, and we design quality estimators for three different analytics units (face recognition, person detection and face detection).
- (3) We propose a reinforcement learning method to automatically, and dynamically tune the configurable parameters of a complex sensor to yield consistent, high-quality insights. To our knowledge, this is the *first* approach to automatically, and dynamically tune camera parameters to enhance specific analytics tasks.
- (4) To significantly speed-up reinforcement learning, we propose virtual knobs and virtual camera models that mimic essential characteristics of a camera; these virtual models are used in reinforcement learning in lieu of a real camera to quickly learn a good reinforcement learning model, and the learnt model is fine-tuned using a real camera in a real-world deployment. Our dynamic tuning approach results in up to 12% improvement in the accuracy of insights from several video analytics tasks.

2 MOTIVATION

Figure 2 shows the processing pipeline within a camera. Photons from the external world reach the image sensor through an optical lens. The image sensor uses a bayer filter [5] to create the raw-image

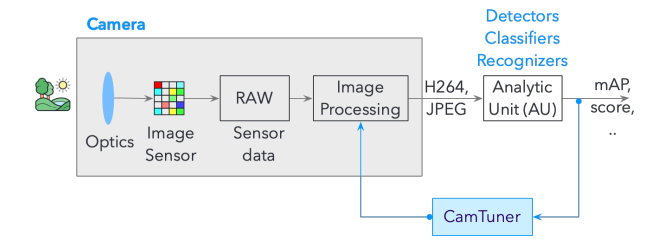


Figure 2: CamTuner Overview

data, which is further enhanced by a variety of image processing techniques [35] like demosaicing, denoising, white-balance, color-correction, sharpening and image compression (JPEG/PNG or video compression using H.264 [4], VP9 [2], MJPEG, etc.) before the image or video is retrieved from the camera. The camera manufacturer exposes many parameters that can be set to control the image generation process. To illustrate the proposed dynamic tuning approach, we consider four popular parameters that are common to almost all cameras: brightness, contrast, color-saturation (a.k.a colorfulness) and sharpness. Please note that other camera parameters can also be dynamically tuned using the *CamTuner* system.

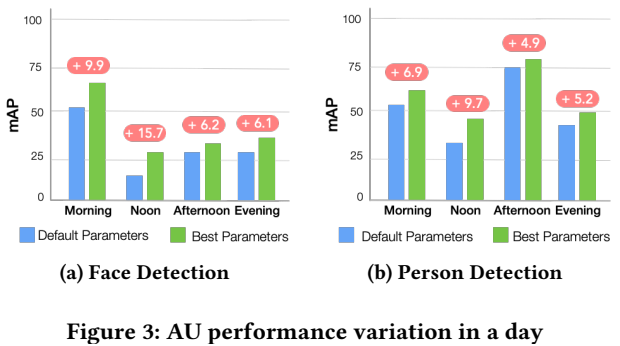
Environmental conditions do change during a day, and these changes affect the quality of images and videos retrieved from the camera. There are no publicly available video datasets that capture the environmental variations in a day by using the same camera (and location). Therefore, we use several videos from our customers to study the impact of these variations on image quality and the insights derived. These videos were captured by camera that was stationary, and the field of view was fixed for the entire length of video capture. For these videos, we also have labelled ground-truth information for several analytics tasks like face detection and people detection. We use RetinaNet [14] to detect faces, and EfficientDet-v8 [43] to detect persons. In both cases, we compare the analytics results with the ground truth information to measure the accuracy of insights from the AUs (we compute the mean Average Precision, or mAP, by using pycocotools [10]).

Figure 3(a) shows the mAP values for the face detection AU during four different times of the day: morning, noon, afternoon, and evening. For the default camera parameter settings, we see that the mAP values vary as the day progresses (blue bars). Therefore, changes in environmental conditions do affect the quality of the frames retrieved from the camera, and this in turn affects the accuracy of insights that are derived from the video data. The green bars show the mAP values when we modify four virtual knobs (as explained in Section 3.1 and Section 3.2) i.e. brightness, contrast, color-saturation and sharpness of each frame as the day progresses. In fact, for each frame, we exhaustively try all combinations of brightness, contrast, color-saturation and sharpness, and select the combination that yields the best analytics results. We use the best combination to modify the frame, and use this modified frame for analytics processing. As shown in the Figure, the mAP values for the green bars are higher than the mAP values for the default settings (blue bars). We observe a similar trend in Figure 3(b) that shows the mAP values for the person detection AU. We note that by varying the four parameters, we observe a 6.1-15.7 mAP improvement for

face detection AU (Figure 3(a)). For the person detection AU, which tries to detect the whole person rather than just the face, we observe a mAP improvement of 4.9-9.7 (Figure 3(b)).

Empirical data in Figure 3 suggests that there is scope to tune the four camera parameters to improve the image capture process, and enhance the accuracy of insights derived. Now, to see this in action with a real camera, we simulate DAY and NIGHT condition in our lab and see the performance of face-recognition AU pipeline described in [38]. In our setup, we use two sources of light and keep one of them always ON, while the other one is manually turned ON or OFF. When both the light sources are ON, it is bright, thereby simulating DAY condition, while when one of them is OFF, it is low-light, thereby simulating NIGHT condition. We place face cutouts of 10 unique individuals in front of the camera and run face recognition pipeline which recognizes these faces. We run this pipeline for various camera settings and for different face matching threshold for the face recognition AU, and measure the Recall ¹ i.e. true-positive rate [49], which is a ratio of number of faces correctly recognized (true-positive) by the AU and the total number of faces in the ground truth. Figure 4a shows the Recall for DAY condition for various thresholds, while Figure 4b shows the Recall for night condition for various thresholds. In both cases, the "Default" settings is where the four camera parameters are set to the manufacture provided default values, while the "Best" settings is obtained by programmatically changing the four camera parameters using VAPIX API [11] provided by camera vendor, and finding the setting that gives the highest Recall value. We vary each parameter from 0 to 100 in steps of 10 and capture frame for each camera setting. This gives us ≈ 14.6 K frames for each condition i.e. DAY and NIGHT. To change one camera setting, it takes about ~ 200 ms through VAPIX API and it took about 7 hours to capture the frames for each condition. We see that the Recall for "Default" setting for DAY condition goes down at higher thresholds, indicating that some faces were not recognized, whereas for NIGHT condition, the Recall remains constant at a low value for all thresholds, indicating that some faces were not being recognized in the "Default" setting. When we actually changed the camera parameters for both conditions and obtained the "Best" setting, we see that we are able to achieve the highest Recall i.e. 1, indicating that all the faces are correctly recognized. This shows that it is indeed possible to improve AU accuracy by changing the four camera parameters.

Please note that modifying camera parameters to capture a better image is fundamentally different from applying transformations on the frames retrieved from the camera. For example, if the image captured by the camera is sufficiently poor due to sub-optimal camera settings, then no further transformations of the video stream from the camera can improve the accuracy of analytics. As shown in Figure 5, we intentionally changed the default camera parameters to certain sub-optimal settings denoted by S1, S2, S3 and S4 and measured the Recall for face recognition AU as before. In these settings, the frames from the camera are of poor quality and we show the Recall for various thresholds, which is quite low for all the settings. Then, we apply digital transformation on these using virtual knobs (as explained in Section 3.1 and Section 3.2) and note the highest



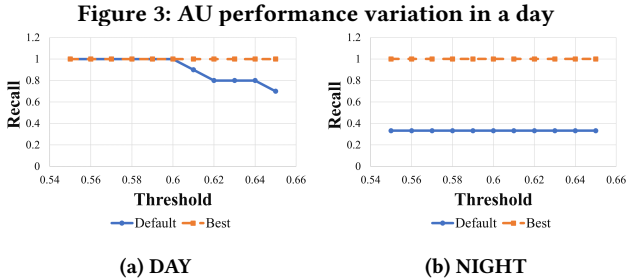


Figure 4: Parameter Tuning Impact for Face-recognition AU

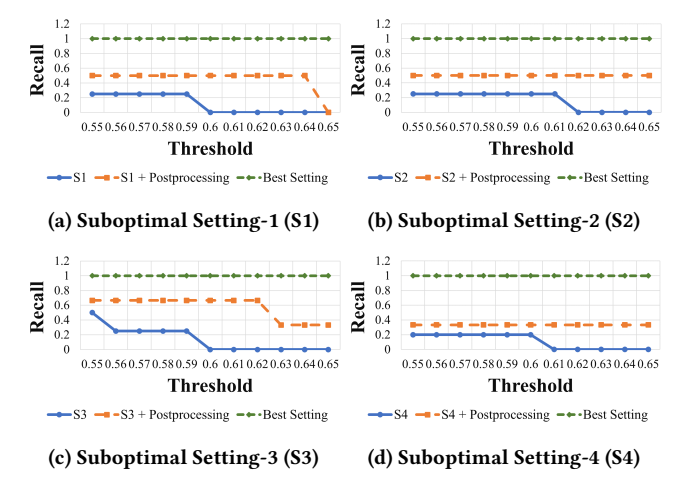


Figure 5: Parameter Tuning vs Postprocessing for NIGHT

Recall value that we can obtain. We see that the Recall improved, compared to the original setting, but it is still quite low. This is because, due to the sub-optimal camera settings, the frames from the camera do not have adequate information about the scene being captured. Now, if we directly change the actual camera parameters, shown by "Best setting", then we are able to achieve the highest Recall i.e. 1. Since we are already achieving the highest possible Recall value, applying further digital transformation on this will not help any further. This shows that modifying camera parameters is fundamentally different from applying transformations on the frames retrieved from the camera.

3 IMPACT OF CAMERA SETTINGS ON AU

We analyze the impact of camera settings on the accuracy of insights from AUs. This will require that we apply different camera parameter settings to the same input scene, and evaluate the impact

¹This face-recognition AU is very good in telling apart face-images that are not of same person. Therefore, high precision is obtained and it remains almost same for different environments, and hence we focus only on Recall.

on the accuracy of insights from AUs. One option is to use multiple cameras with different camera parameter settings to record the same input scene. However, there are thousands of different combinations of just the four camera parameters that we focus on in this paper, and it is impractical to use real cameras to analyze the impact on AUs. Therefore, we propose *Virtual knobs*, which are digital equivalents of the camera parameters, to analyze the impact of camera parameter changes on the accuracy of insights. Section 3.1 describes the design of virtual knobs.

3.1 Virtual knobs

Our goal is to design proxies for the four camera parameters. We use a camera and an image transformation algorithm in the Python Imaging Library [1] to design the virtual knobs.

Algorithm 1 describes our method to establish a correspondence between parameter values of the image transformation algorithm (which are the virtual knobs), and camera parameter values. Establishing such a correspondence is quite useful. For example, given an image, the image transformation algorithm can be used to create many modified images (by applying different combinations of the four parameter values). Then, modified images can be processed by the analytics unit to identify a combination of values (of the four parameters) that yields the best analytical results, and this combination can be mapped back to a set of camera parameter values by using the correspondence. So, by applying the correspondence, we can determine good values for the camera parameters, and for these camera parameter values, the frames produced by the camera will result in highly accurate insights from the analytics unit.

We determine the correspondence between the parameter values of the image transformation algorithm, and the camera parameters, as follows. We set the camera parameters to their mid-range, or as recommended by the camera manufacturer, and we capture an image im. Algorithm 1 has an outer loop where we progressively change the camera parameter values (through the range of values supported by the camera vendor for each camera parameter) and generate different images im_p for a static scene. For each image im_p , which corresponds to a particular camera parameter setting, the inner loop determines the closest set of parameter values of the image transformation algorithm that will produce a modified image im_d that has the same image quality as im_p . These set of parameter values of the image transformation algorithm (i.e. the virtual knobs) now correspond to the specific camera parameter settings that generated the image im_p . By repeating the above procedure, we determine the correspondence between different camera parameter settings and the different parameter values of the image transformation algorithm.

We use de-facto full-reference image-quality assessment metric, structural similarity (SSIM) [46] to match the image quality of im_p (image from camera) and im_d (modified image produced by the image transformation algorithm). For example, if the SSIM value for the pair (im_p , im_d) is higher than 0.9, then the image from the camera and the modified image from the image transformation algorithm are both of good visual quality [12]. Table 1 shows the range for the virtual knobs that correspond to the full range of camera parameter settings (usually, between 0 and 100).

Algorithm 1: Camera Parameter-to-Virtual Knob Mapping

```
Input: Virtual Knob Values dval_{list};

Camera Parameter Values pval_{list};

1 Obtain im with default camera parameter value pval_{default};

2 for p in pval_{list} do

3 | Obtain im_p from the camera changing camera parameter to p

for d in dval_{list} do

4 | im_d \leftarrow \text{Augment } (im_d);

5 | ssim\text{-val}(d) \leftarrow \text{SSIM } (im_p, im_d)

6 end

7 | d_{virtual} \leftarrow \text{arg } \max_d ssim\text{-val}(d)

8 | return (p, d_{virtual})

9 end
```

Tuning-param	Range of virtual knob
Brightness	[0.6, 1.6]
Contrast	[0.6, 3.6]
Sharpness	[0.5, 1.6]
Color-Saturation	[0.1, 2.0]

Table 1: Virtual Knob Ranges

3.2 Impact of varying virtual knobs

We analyze the impact of changing the values of virtual knobs on the accuracy of insights from the analytics units. We consider images and video snippets from popular public datasets. These images and videos were captured under different environmental conditions, and by different cameras with unknown camera settings. Our analysis (a) quantifies the possible improvement in the accuracy of insights by tuning virtual knobs, (b) demonstrates that different camera parameter settings are desirable for different environmental conditions, and (c) identifies the specific camera parameter setting that can enhance the accuracy of insights from the analytics unit.

3.2.1 Static images. We consider images in public datasets like Fivek RAW dataset [6] and celebA [29]. These images were taken using different cameras, and under different environmental conditions. For each image, we determine the best combination of virtual knobs that results in the most improvement in accuracy of insights from the analytics units.

Person and Face Detection AUs: We use efficient detection AU, and perform analytics on a random subset of 100 Fivek raw images. First, we manually annotated the 100 images to detect persons and the bounding boxes for their faces using cvat-tool [32]. This is the ground truth. Then, for each AU, we used Algorithm 2 to identify the best combination of virtual knobs for the AU by using a combination of mAP and true-positive IoU 3 as the analytical quality metric. When we use the best combination of virtual knobs for each image, and modify the image using this combination of values for the four parameters, the AU performance improves. For example, the face detection AU detects faces in $39~\mathrm{more}$ images when compared with face detection on the original 100 images. The

 $^{^2}$ input-size of efficient det-v0 closely matches with the raw image resolution while compared with other efficient det variants.

³where single bounding box prediction for a object with IoU>0.5 with correct classification

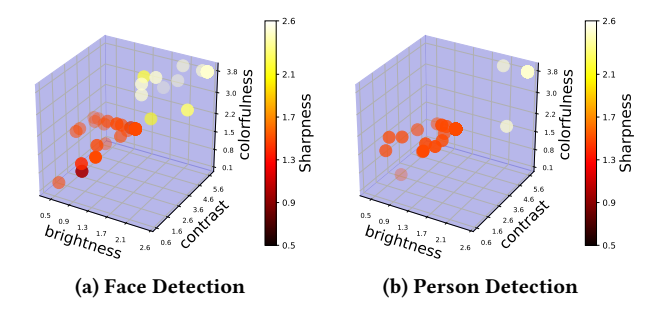


Figure 6: Distribution of best configurations for different AU on fivek raw-dataset

distribution of the best virtual knob combination for each image is shown in Figure 6. Each point in the figure corresponds to an image in the subset of 100 Fivek images, and the coordinates of the point are the best virtual knob combination for the image ⁴. Clearly, the best combination of virtual knobs for each image are not clustered, suggesting that a single, fixed camera parameter setting is not ideal.

Algorithm 2: Find Best Configuration for Detection

- 1 for i in confs do
 - $im_{aug} \leftarrow \text{Augment}(im,i);$
- $3 \mid dets \leftarrow AU(im_{aug});$
- a mAP, true-positive IoU ← mAP (dets, gt) with 0.5 iou-threshold;
- 5 end
- 6 First Sort *confs* using corresponding mAP;
- 7 Then for same top-1 mAP *confs* sort using true-positive IoU;
- ${f 8}$ return top-1 conf from final sorted list

Face Recognition AU:. We use the face-recognition AU pipeline described in [38]. We use one face image of each person in the CelebA dataset to populate the pre-defined gallery of face images, and use the remaining face images as queries. The analytical quality metric for face-recognition AU is the true-positive match-score. We use Algorithm 2, and this quality metric, to determine the best virtual knob configuration for each person in the 300-person CelebA dataset. When we modify the query images by using their best virtual knob settings, then face-recognition AU recognizes 41 more face-images correctly when compared to recognition on the original query images (faces in 256 original images are correctly recognized). Moreover, best virtual knob configuration for each query image improves the average true-positive match-score by 3.6% (e.g., maximum AO improvement 11.6%). The distribution of the best virtual knob combination for each query image is shown in Figure 7. Again, each point in the figure corresponds to an image in the 300-person CelebA dataset, and the coordinates of the point are the best virtual knob combination for the query image. Clearly, again, the best combination of virtual knobs for each image are not clustered, suggesting that a single, fixed camera parameter setting is not ideal.

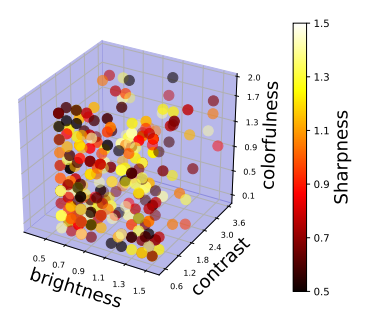


Figure 7: Distribution of best configurations for face-recognition AU on CelebA

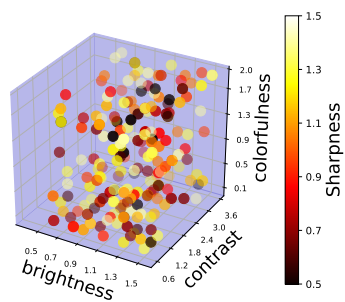


Figure 8: Distribution of best configurations for facial-KP AU on 300W

Facial Keypoint Detection AU: Facial keypoint detection AU [23] detects 68 facial landmarks in a face. We use images from the 300W dataset [37]. Analytical quality metric for this AU is the root-mean-square (RMS) distance between the predicted and actual landmarks ⁵. If we modify each image by using its best virtual knob configuration, then the facial-keypoint detection AU detect facial landmarks in 11 more images. Also, for the 215 images where facial landmarks were detected by the AU by using the original images, the analytical quality of their corresponding, modified 215 images improved by an average of 31.1%. This shows that camera parameter tuning generally improves the analytical quality of all images. Figure 8 shows the distribution of the best combination of virtual knob values for all the images in the 300W dataset, and again, the best virtual knob configurations do not cluster. Therefore, a single, fixed camera parameter setting is not ideal.

3.2.2 Video snippets. We analyze the impact of virtual knob settings when analytics are performed on videos. We consider 19 video snippets from HMDB dataset [26] and 11 video snippets from Olympics dataset [30]. Similar to the images case, we manually annotated the face and person bounding boxes. This is our ground truth. Each video-snippet contains no more than a few hundred frames, and the environmental conditions for a video are largely constant. However, the environmental conditions appear to vary across the video snippets. We determine one best combination of virtual knobs for each video. Figure 9 and Figure 10 show the distribution of the best virtual knob combinations for the 19 videos in the HMDB dataset and the 11 videos in the Olympics dataset, respectively. Again, the best virtual knob combinations for each

⁴We first use the virtual knob range shown in Table 1, but since we observed that the best configuration is towards the upper-limit of those ranges, we extended the virtual knob range to make sure we are not missing out on other possible best configuration.

 $^{^{5}}$ low RMS distance implies better analytical quality

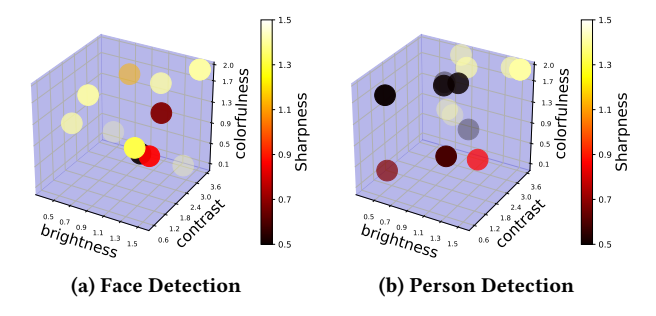


Figure 9: Distribution of best configurations for different AUs on *HMDB* video snippets

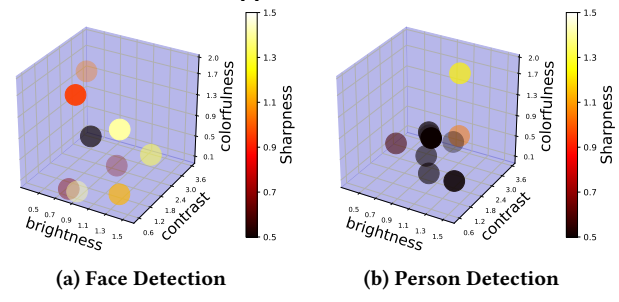


Figure 10: Distribution of best configurations for different AUs on *Olympics* video snippets

video in a dataset do not cluster (although there are a few of them that overlap), suggesting that a fixed camera parameter setting is not ideal for different environmental conditions or analytics tasks.

Table 2 shows the maximum and average analytical quality improvement achieved after tuning each video-snippet as per their best virtual knob configuration. We observe that up to 58% improvement in accuracy of insights is possible when camera parameters are modified appropriately.

Video-Dataset	AU	mAP	
		improvement	
		Max	Mean
Olympics	Face Detection	19.23	1.68
	Person Detection	40.38	8.38
HMDB	Face Detection	18.75	4.22
TIMDB	Person Detection	57.59	12.63

Table 2: Best configuration Accuracy Improvement

The camera parameter settings that provide the best improvement in accuracy of insights from analytics units are impossible for a human to identify because the best combination will vary with location of the camera, the type of analytics units, and the environmental conditions. Humans cannot keep adjusting these parameters manually, and methods to automatically and dynamically tune camera parameters are required to improve the accuracy of insights from analytics units. We describe such a system in the next section.

4 SYSTEM DESIGN OF CamTuner

Figure 11 describes the system-level architecture for automatic, and dynamic tuning of camera parameters. Live video streams from

the camera are processed at the edge by a lightweight AQuA module [33] to discard low-quality frames. These frames are not suitable for analytics, and early discard helps to reduce the required wireless network bandwidth. At the edge of the wireless network, the video stream is mined for insights by using analytic units. An AU-specific analytics quality estimator detects a change in analytics quality, if any, and communicates with a reinforcement learning module that dynamically, and remotely, adjusts the camera parameter settings.

Detecting a change in accuracy of insights from the analytics unit is a difficult task. Since no ground truth is available during normal operation of the streaming system, we design a proxy that estimates the accuracy of insights. Design of the AU-specific analytics quality estimator is described in Section 4.1. A reinforcement learning module reacts to a change in analytical quality estimates, and dynamically adjusts the camera parameters to improve the accuracy of insights. Section 4.2 describes the reinforcement learning module.

4.1 AU-specific analytics quality estimator

As described in Section 3.2, methods to estimate the accuracy of insights from analytics units depend on the function of the analytics unit. For example, a combination of mAP and true-positive IoU is typically used to estimate the accuracy of insights from a face or person detection AU, while true-positive match-score is the preferred analytical quality metric for a face recognition AU. Similarly, a common analytical quality metric for key-point detection AU is the root-mean-square distance between the predicted and actual landmarks. All these analytical quality metrics assume availability of ground-truth, which is compared with the predicted outputs from the analytics units.

Since no ground truth is available in a real-world deployment, we need a different approach to estimate analytical quality. We propose training a deep-learning model to predict analytical quality estimates for an analytics unit. We trained two different AU-specific analytical quality estimators, and we briefly describe these models.

• Estimator for Face-recognition AU: For 300 randomly-sampled celebrities from celebA dataset [29], we choose two images per person. We use one of them as a reference image and add it to the gallery. We use the other image to generate multiple variants by changing the virtual knob-values. These variants are the query images (≈ 4M query images). For each

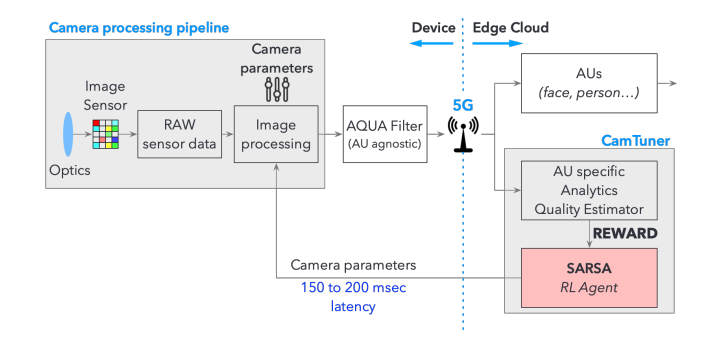


Figure 11: CamTuner System design

query image, we obtain the match score (which is a value between 0 and 1) by using the Face recognition AU. The query images along with their match score are the labeled examples we use to train a deep-learning model, which will predict the match score for an image. We trained a deep-learning model (network architecture is similar to the lightweight AQuA network) with 101 output classes. One of the classes signifies no match, while the remaining 100 classes correspond to a match score between 1 to 100.

• Estimator for person & face detection AU: We used Olympics [30] and HMDB [26] datasets, and created ≈ 7.5M variants of the video frames. Then, we used the AUs to determine the analytical quality estimate, which is a combination of mAP and IoU values (as shown in Equation 1). The video frames, and their quality estimates, are the labeled examples, and we trained a deep-learning model (again, the network architecture is lightweight and similar to AQuA network) with 201 classes to predict the analytical quality estimate for a video frame.

$$classlabel \leftarrow mAP + IOU_{True-Positive} * 100$$
 (1)

4.2 Reinforcement Learning

To automatically tune the camera parameters, we use reinforcement learning (RL) [41] techniques. We use State-Action-Reward-State-Action (SARSA) RL algorithm [47]. In this setup, there is an agent, which interacts with the environment (*state*) it is in, by taking different *actions*. As the agent takes actions, it moves into a new state or environment. For each action, there is an associated *reward* or penalty, depending on whether the new state is desirable or not Over a period of time, as the agent continues taking actions and receiving rewards and penalties, the agent learns to maximize the rewards by taking the right actions, which ultimately leads the agent towards desirable states.

SARSA does not require any labeled data or pre-trained model, rather it learns and updates its policy based on the action it takes. Therefore, it is an on-policy learning algorithm and requires a clear definition of the environment (state), actions and reward. For the purpose of automatic camera-parameter tuning, we define them as follows:

<u>State</u>: This is a vector containing (a) the current brightness, contrast, sharpness and color parameter values on the camera and (b) measure of brightness, contrast, sharpness and color-saturation.

<u>Action</u>: The set of actions that the agent can take are (a) increase or decrease one of the brightness, contrast, sharpness or color-saturation parameter value or (b) not take any action at all.

<u>Reward</u>: We use the AU-specific analytics quality estimators as the reward function for SARSA algorithm. If the quality estimate improves, then it is considered as a reward, whereas if the estimate decreases, then it is considered as a penalty.

The reward obtained by using the proxy analytics quality estimator is termed as the immediate reward. Along with considering immediate reward, the agent also factors in future reward that may accrue as a result of the current actions. Based on this, a value, termed as Q-value is calculated for taking an action a when in state a. This is denoted as a0, a1. The value for a2, a3 is calculated as

Algorithm 3: State-Action-Reward-State-Action loop

```
1 s \leftarrow Observe-Environment()
2 a \leftarrow Choose-Action(Q, s)
3 while Still-Processing() do
4 | Perform-Action(a)
5 | r \leftarrow Compute-Reward()
6 | s' \leftarrow Observe-Environment()
7 | a' \leftarrow Choose-Action(Q, s')
8 | Q(s, a) \leftarrow Q(s, a) + alpha \times [r + gamma \times Q(s', a') - Q(s, a)]
9 | s \leftarrow s'
10 | a \leftarrow a'
11 end
```

per Equation 2. Here, α is a constant with a value between 0 and 1. This can be used to control how much importance is to be given to new information obtained by the agent. A value of 1 will give high importance to the new information while a value of 0 will stop the learning phase for the agent. During the initial phase, a higher value e.g. 0.9 can be assigned by the operator, which will help the agent quickly *learn* and understand the new environment by giving higher importance to the most recent information. After the agent has learnt and assimilated the information from the new environment, the value of α can be lowered e.g. 0.1 by the operator so that the agent now starts using the gathered information about the new environment.

$$Q(s,a) \leftarrow Q(s,a) + \alpha \left[r + \gamma \cdot Q(s',a') - Q(s,a) \right]$$
 (2)

Similar to α , there is another constant γ in equation 2, which has a value between 0 and 1. This constant is called as the discount factor and can be used to control the importance given by the agent to any long term rewards. A value of 1 will give very high importance to long term rewards while a value of 0 will make the agent ignore any long term rewards and focus only on the immediate rewards. If the conditions change very frequently then a lower value e.g. 0.1 can be assigned to γ so as to prioritize immediate rewards, while if the conditions do not change frequently, then a higher value e.g. 0.9 can be assigned to prioritize long term rewards.

The steps followed by an agent are shown in Algorithm 3. Here, the agent first observes the environment i.e. state s and chooses an appropriate action a to be performed in state s. After performing the action a, the agent receives an immediate reward (or penalty) r and is now in a new state s'. In this new state, the action chosen by the agent is a' and the associated Q-value is Q(s', a'), which the agent uses to compute the cumulative reward Q(s, a) as per equation 2. The agent then updates this computed cumulative Q-value and is now in the new state s'. This process continues for the lifetime of the AU as the agent continuously learns and adapts to the environment.

While algorithm 3 provides the steps followed by the agent, it does not provide the exact method used by the agent to choose the action *a* to be performed. For this, we devise a *new* policy for the agent to decide the action to be performed. This policy is shown in algorithm 4. We define a constant called *epsilon* which has a value

Algorithm 4: Policy for choosing the action to perform

```
Input:Q,s,a,r
1 if rand(0,1) ≥ epsilon then
2 | return Random-Action()
3 end
4 if r < 0 then
5 | return Revert(a)
6 end
7 a' ← Max-Action(Q, s)
8 if r > Q (s,a') then
9 | return a
10 end
11 return a'
```

between 0 and 1 and can be tweaked by the operator. Initially, the agent generates a random number between 0 and 1. If the random number is greater than the set value of *epsilon*, then a random action is chosen. As we can see, lower value of epsilon will trigger more random actions to be generated while higher value of epsilon will trigger less random actions. Therefore, during the initial phase of the deployment, when the agent explores various actions, typically the value of epsilon is set lower e.g. 0.1, while after the agent has explored enough, the value of epsilon is set higher e.g. 0.9, so that the agent starts using the learned information from the earlier exploration phase and starts exploiting it. If the random number is lower than the set value of *epsilon* then the reward *r* is checked. If the reward is less than 0 i.e. if the action results in a penalty, then the action is reverted immediately. However, if the reward is positive but less than the predicted reward for the action, then the same action is repeated. Thus, this is a greedy policy where the actions leading in positive direction are repeated while the action leading in negative direction are immediately reverted.

It may happen sometimes that due to extremely poor capture from the camera (due to sudden change in environment e.g. lights being turned off in an indoor setting), most of the frames get dropped by AQuA-filter. In such cases, without any frames being sent to *CamTuner*, RL agent will not be able to take any corrective actions. To avoid this scenario, we designed AQuA-filter in such a way, that after every configurable number of successive frames being dropped, 1 frame is sent to AU-specific Analytics Quality Estimator, so that *CamTuner* is aware of actual frames being produced by the camera and can take appropriate action.

5 VIRTUAL CAMERA

5.0.1 Need. RL module, described in Section 4.2, requires the agent to learn by going through different states, taking different actions and correctly interpreting the corresponding reward. This learning process requires that the video feed goes through various environmental changes, so that the model developed is robust. If we work with real cameras, it may take weeks or even months to go through such changes. It is not practical to wait so long to train the model. Besides, it does not give the flexibility to test various reward functions because the conditions are not reproducible and experiments are not repeatable in such a setup. Therefore, we propose a virtual

camera (VC), which mimics a real camera, but it does not have the drawbacks of working with a real camera to train the RL module. VC allows us to (a) conduct experiments where various camera parameter configurations can be applied to the exact same scene, which enables us to have repeatability and reproducibility in our experiments (note that this is not possible with a real camera), (b) run the experiments much faster than real-time; we can process video frames at a much higher frame rate like 300 frames per second rather than the 25-30 frames per second from a real camera, and (c) independently test and train RL algorithms with various reward functions. Along with these, in scenarios where there are multiple AUs running on a single video feed, it may happen that each AU requires a different "best" camera setting. However, it is not possible to have separate camera settings for each AU, since there can be only one camera setting at any given point in time. In such scenarios, VC can be used by each AU and custom "best" camera setting can be simulated through VC as per specific AU requirements [20].

5.0.2 Design. In order to mimic a real camera, VC accepts a prerecorded video and the time of the day as input. Based on the time of the day and current VC camera parameters, which we refer to as virtual knobs, VC applys transformation on the frames and produces the final image. Note that VC exposes APIs, similar to a real camera, to change the virtual knobs. Fig. 12 shows *CamTuner* system design with VC, where the RL agent changes the virtual knobs and learns much quickly using such a setup with VC. VC design consists of two phases: (a) offline profiling phase, (b) online phase.

Offline profiling phase: This phase consists of two parts. First, to obtain a mapping between time of the day and the corresponding feature tuple (consisting of brightness, contrast, color-saturation and sharpness values) for that time. Second, to obtain a mapping between delta change between two feature tuples and the corresponding virtual knob value. These mapping tables are used in online phase to render the frame by VC.

Algorithm 5 shows the procedure to obtain the mapping between time of the day and corresponding feature tuple. We refer to this mapping as VC table. To generate this VC table, we use a full 24 hour long video which is broken into 5 minute video snippets. The VC table that we generate has a granularity of 15 minutes i.e. for a period of 15 minutes, we have a corresponding feature tuple. Thus, we have total 96 intervals in a 24 hour period and for

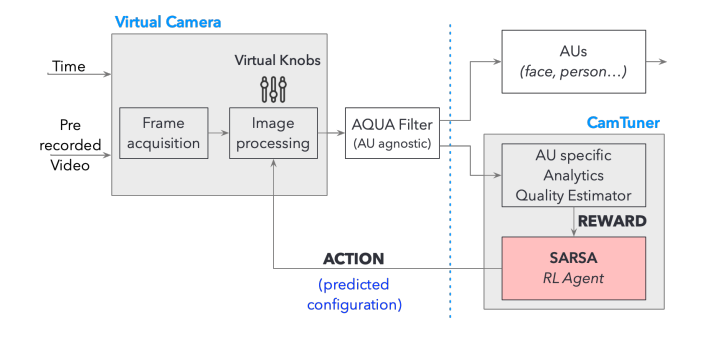


Figure 12: CamTuner system design with VC

Algorithm 5: VC Table Generation

each tile for each 15 minute interval

frames for a specific tile

```
Input :5-minute video-snippets V_S;
   // divide 24 hours into 96 equal intervals, each being
      15 min long (intvl)
1 for index in range(0,96) do
       for V_S with capture-timestamp \in intvl_{index} do
2
           frames \leftarrow DecodeFrames (V_S)
 3
           for frame in frames do
 4
               // split each frame into 12 tiles
               tiles ← SplitFrame (frame)
 5
               // featureTuple←<brightness,contrast,color,sharpness>
               for tile in tiles do
                   featureTuple_{tile} = ExtractFeatures (tile)
 7
 8
               end
           end
       end
10
         compute mean feature values across all videos
          captured with 15 min
       Compute Mean Value featureTuple intvl
11
12 end
13 return 12 tables storing Mean feature Tuple _{tile}^{intvl} corresponding to
```

Algorithm 6: Delta-change to Configuration mapping Table Generation

```
Input:5-minute video-snippets V_S; r_B, r_{Con}, r_{Col}, r_S are virtual
              knob ranges obtained from Table 1;
   // each 15 min interval, intvl
1 for randomly selected Frame from each interval do
        for tile in range(1,13) do
             // featureTuple←<brightness,contrast,color,sharpness>
             \texttt{featureTuple}_{tile}^{org} \leftarrow \texttt{ExtractFeatures}\left(frame_{tile}\right)
             for virtual_{conf} \in (r_B \circ r_{Con} \circ r_{Col} \circ r_S) do
 4
                  // <Bright, Contrast, Color, Sharp> ←
                  virtFrame_{tile} \leftarrow RenderFrame (Frame_{tile},
                    virtual_{conf})
                  featureTuple_{tile}^{virt} \leftarrow \texttt{ExtractFeatures}
                    (virtFrame_{tile})
                  // compute delta changes after re-rendering
                  \text{delta[0]} = \frac{featureTuple_{tile}^{virt}[0]}{featureTuple_{tile}^{virg}[0]}
 7
                  compute delta[1], delta[2], delta[3] for 3 other knobs
 8
                  Store <delta> corresponding to virtualconf
 9
10
             end
        end
11
12 end
   Compute Median <br/> <br/>delta> for same virtual_{conf} across sampled
```

each interval, we have 3 video snippets. We go through each of these video snippets, extract the frames, and for each of the frames, we divide the frame into 12 tiles (to account for variation in local feature values in different parts of the frame, as shown in Figure 13), and for each tile, we obtain the corresponding feature tuple

14 return 12 <delta>-vs-configuration Mapping tables for each tile

Algorithm 7: Runtime VC Simulator

```
Input :input frame corresponding to time T1, inpFrame T1; Out-
               put Time T2;
   Output: input frame corresponding to output time T2, inpFrame T^2;
   // split input frame into 12 tiles
 \text{1 inpFrame}_{tile}^{T1} \leftarrow \text{SplitFrame}\left(\text{inpFrame}^{T1}\right)
2 for tile in range(1,13) do
         // featureTuple←<brightness,contrast,color,sharpness>
         // Measure input frame features
         \texttt{featureTuple}_{tile}^{T1} \leftarrow \texttt{ExtractFeatures} \ (\texttt{inpFrame}_{tile}^{T1})
         // obtain features corresponding to output time
         Get feature
Tuple ^{T2}_{tile} from VC-table 5
         // compute delta change from T1 to T2 for 4 knobs
        \text{delta[0]} = \frac{featureTuple_{tile}^{T2}[0]}{featureTuple_{tile}^{T1}[0]}
 5
         Similarly obtain delta[1], delta[2] and delta[3]
         config ← FindClosestMap (<delta>) using L1 norm distance
          and table generated in Alg 6
         append config to a configList
9 end
\textbf{10} \ \operatorname{config}_{median} \leftarrow \operatorname{GetMedian} \left( \operatorname{configList} \right)
11 inpFrame<sup>T2</sup> \leftarrow RenderFrame (inpFrame<sup>T1</sup>, config<sub>median</sub>)
```

(variation of these different features across entire day for each tiles is shown in Figure 14). We then compute the mean for each tile for a 15 minute interval. This forms the VC table, with feature tuple values for each tile for each 15 minute interval, as shown in Figure 15a.

Algorithm 6 shows the procedure to obtain the mapping between delta change between two feature tuples and the corresponding virtual knob value. As in Algorithm 5, we use a full 24 hour long video which is broken into 5 minute video snippets. As before, we use a granularity of 15 minutes as our interval and select a random frame within an interval to form a collection of frames with varying conditions. Again, for each of these frames, we consider separate tiles (total 12) and for each of the tile, we extract the feature tuple (original). Now, using the ranges obtained from Table 1, we generate all combinations of the possible virtual configurations, and for each of those configurations - we render the frame using the specific virtual configuration, extract the feature tuple on the rendered frame and then compute the delta change between the original and rendered frame for each of the feature tuple. This forms a mapping between the delta change and the corresponding virtual configuration. Now, we have such mapping for each of the randomly selected frames and for each tile. Lastly, we combine the delta values across all frames by taking the median and generate a table, called VC delta-change table, consisting of mapping between the delta change and corresponding virtual configuration value, for each tile, as shown in Figure 15b.

Online phase: During *online phase*, VC actually transforms the pre-recorded input video (of time T1) to any other desired time of the day (T2), provided as input. Algorithm 7 shows the procedure followed by VC to perform this transformation. Each input frame of time T1 is first split into 12 tiles. Then, for each tile, feature tuple is extracted. Then, for the desired time T2, the corresponding feature tuple is obtained from VC table (output from algorithm 5).



Figure 13: Tiled representation of a captured frame

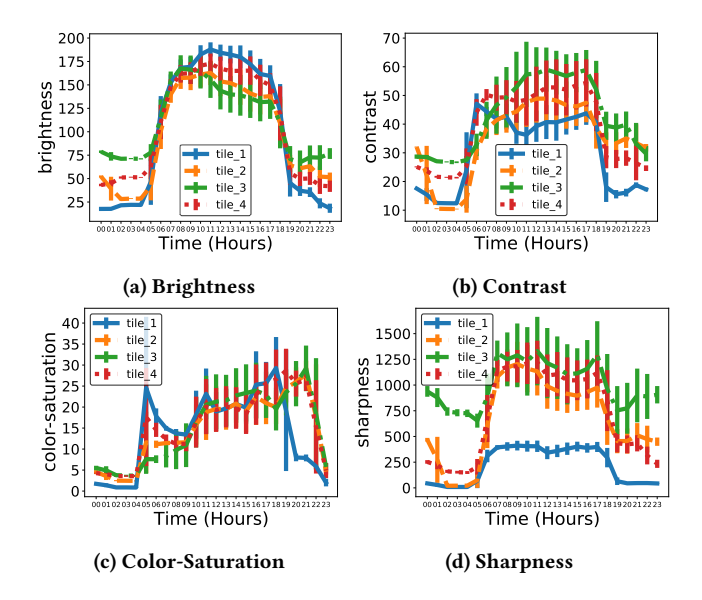


Figure 14: Day-long feature profiles for different tiles

Delta change between the feature tuple at time T2 and time T1 is then computed. The virtual configuration values corresponding to the closest delta change (using L1 norm distance [48]) is obtained from VC delta-change table (output from algorithm 6). Once the configuration is obtained for each tile, a median configuration is computed across tiles (to eliminate visibility of distinct tiles in the frame) and this configuration is used to render the frame for time T2. Thus, the frame at time T1 is transformed by VC to a frame at time T2.

While training the RL module, as shown in Figure 12, RL agent uses the APIs exposed by VC to change the virtual knob values and learns much quickly, as (a) different environmental conditions can be generated easily by VC (b) frames can be processed at a much faster rate, even up to 300 FPS, by using more computing hardware, and (c) virtual knob values can be changed instantly.

6 EVALUATION

We discuss our evaluation methodology and describe our performance evaluation results for the three main components: virtual camera, AU-specific analytics quality estimator and SARSA RL agent. We then analyze the overall system performance through a real-world deployment.

Time of day	Feature-Values	
10:00	<159,53,11,2122>	
10:15	<160,52,13,2100>	

Delta Change	Virtual Knob Confs
<0.5,0.7,1.5,2>	<0.7,0.6,1.1,1.2>
<10,18,5,9>	<1.5,2.4,1.6,1.5>

(a) VC Table

(b) Delta-to-Configs Table

Figure 15: Offline Generated Tables

6.1 Evaluation methodology

We loop a pre-recorded (original) video through two virtual cameras. For the first virtual camera, we gradually change the model parameters to simulate the changes that happen during the day as the sun changes its direction and finally sets. This way, the video feed coming out from the first virtual camera mimics the conditions that would have occurred as the lighting changes from daylight to evening, to twilight, to dusk and finally night. Under this gradual change in light conditions, we continuously measure the accuracy of the insights from the AU. The first virtual camera is not controlled by the RL module, and results from the first virtual camera video feed are our baseline. For the second camera, we also gradually change the model parameters to simulate the lighting changes that would have occurred during the day, but on this second virtual camera, we also adjust the virtual knobs dynamically by using our reinforcement learning module. Then, we compare the accuracy of insights from the AU to the baseline results.

Note that in our experiment, it is important to choose a good quality video as original video. If we start with a poor quality video (for example, night video with poor lighting), then the output video from the virtual camera does not have enough information; so no matter how much we adjust the virtual knobs, it wouldn't help. This jives with the fact that in actual deployment, our technique would constantly monitor the conditions and keep tuning camera parameters (from daylight all the way to night) so that the camera feed is of reasonably good quality at all times. By using our technique, we avoid the situation where the video feed coming out of the real camera is of exceptionally poor quality.

6.2 Training

We train AU-agnostic AQuA-filter by using the lightweight inception-v3 [42] backbone until the first inception block ⁶ by using the validation images from ImageNet ILSVRC-2017 dataset [13] and their augmented variants. Along with 7 different distortions mentioned in [33], we also train AQuA for color-saturation and sharpness variations.

AU-specific analytics quality estimators use a similar network as AQuA. However, these estimators have different number of output nodes (or classes) for different AUs. We use cross-entropy loss function to train AU-specific estimators, while the AU-agnostic AQuA model is trained using MSE loss. All models are trained end-to-end with an initial learning rate of 10^{-5} and we use the Adam Optimizer [24].

⁶AQuA-filter uses only 14% of total model-size of Inception-v3

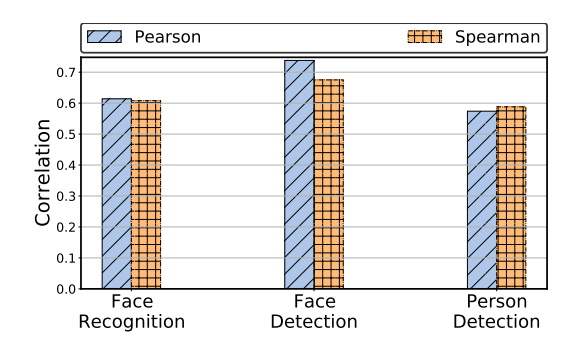


Figure 16: AU-specific analytics quality estimator Performance

6.3 Virtual camera

VC should faithfully render a frame from time T1 to any other time T2, as if it was actually captured at time T2. In order to evaluate if VC is able to do this, we obtain several video snippets at different hours of the day. Then, we run these video snippets through VC and generate 23 other video snippets (for other hours of the day). We then compare the values of feature tuple of the generated video snippets through VC (transformed) and the values of feature tuple from the video snippets actually captured at those hours (original). Table 3 shows error and standard deviation between the transformed and original videos. We note that average VC error is under 20~% for brightness, contrast, color-saturation and sharpness.

Brightness	rightness Contrast Color	Sharpness	
		-Saturation	
5.4 % ± 1.7 %	13.8 % ± 4.3 %	17.3 % ± 9.6 %	19.8 % ± 8.1 %

Table 3: VC error

6.4 AU-specific analytics quality estimator

We evaluate the performance of AU-specific estimators by determining the correlation between predicted quality estimates and the analytical quality estimates derived using ground-truth. Figure 16 shows the Spearman and Pearson correlation metric for three different AUs. The match-score for celebA-validation images with its augmented variants (\approx 2M) and predicted quality by facerecognition-specific analytics quality estimator is strongly correlated (Pearson and spearman correlation both are greater than 0.6) 7 . For face-detection and person-detection quality estimators, we used annotated video frames from olympics [30] and HMDB dataset [26] and their various variants that were generated by changing the virtual knobs. Figure 16 shows the strong positive correlation between the measured mAP and IoU metric, and the predicted quality estimate for both face-detection and person-detection AUs. This strong correlation enables CamTuner's RL agent to tune camera parameters based on the reward value provided by AU-specific analytics quality estimator.

6.5 SARSA RL

We applied SARSA RL agent to tune four virtual knobs in the virtual camera pipeline (as shown in Figure 12) on 5-minute video

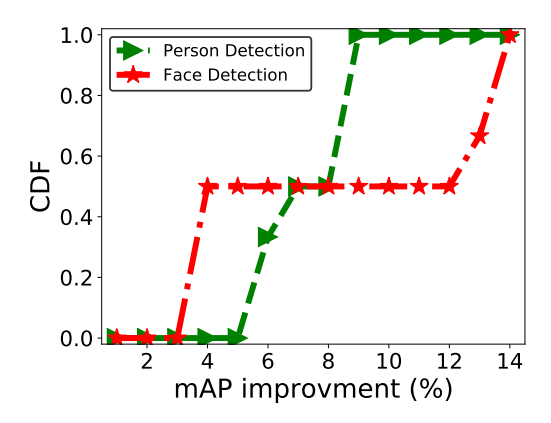


Figure 17: CDF of mAP improvement for different AUs

segment (i.e., consists of 7500 frames) 8 for 6 randomly selected time segments throughout the day (each time-segment is separated by at least 1 hour). RL agent adaptively adjusts the four virtual knobs with the help of AU-specific reward function, as explained in Section 4.1, after every $1 \, min$ interval (this interval is configurable). Figure 17 shows the cumulative distribution function of mAP improvement for the six videos that correspond to six distinct time-segment of the day. Each point (x,y) in Figure 17 shows that y% of videos experience mAP improvement that is between 0 to x%. Dynamically adjusting the four virtual knobs by using RL improves face-detection accuracy by 8.31% on average (the mAP improvement can be as much as 13.74%). Similarly, we notice a 7.35% average mAP improvement for person-detection (the mAP improvement can be as much as 8.95%).

6.6 Overall System Analysis

To ensure repeatability and reproducibility, we use the same scenes to evaluate the performance before and after applying CamTuner. We use a virtual camera and loop-through pre-recorded proprietary videos taken at different time-segments of day, as shown in Figure 12. The virtual camera continuously extracts frames from the input video and applies transformations to re-render it to emulate different time-segments of the day without changing the frame-content (explained in Section 5). Before offloading to edge-server, frames are passed through the AQuA filter. Both Virtual camera model and AQuA model are running on a low-end edge device with tiny footprint, Intel-NUC box equipped with Intel i7-6770HQ 2.6 GHz CPU. AQuA filter takes 40 ms processing time (with a CPU usage $\approx 80\%$) per frame, and outputs a quality value. Depending on this quality value and threshold, inferior-quality frames are discarded and the rest are sent for analytics processing to the edge-server over a 5G network with an average offload latency of 39.7 ms. Temporal locality in captured video helps to offset AQuA computation overhead on edge device by applying AQuA-filter only on a few intermediate frames. AQuA-filter on edge device also helps to reduce the 5G bandwidth requirement by 15%-20%.

On the edge-server, RetinaNet face detection AU, EfficientDet person detection AU and AU-specific analytical quality estimators are running on *NVIDIA GeForce RTX 2070 GPU*. RetinaNet face detection AU takes *86 ms* while person detection AU takes *96 ms* to

 $^{^7\}mathrm{Pearson}$ correlation greater than 0.5 [40] and spearman correlation [44] value greater than 0.6 imply strong correlation.

 $^{^8 \}mbox{Ground-truth}$ annotations are done on the video-segment to find out the actual detection accuracy (mAP) improvement.

process each frame on a GPU (utilization is $\approx 25\%$). Computation time for AU-specific analytical quality estimators is only 14 ms on this GPU server. SARSA RL agent (on an *Intel i9-9980XE 3GHz CPU*) can perform each action within a few milliseconds by using virtual knobs, which otherwise would take several hundred milliseconds on a real camera.

6.7 Real-world deployment

We position two cameras side-by-side so that both cameras view almost same scene at the same time, as shown in Figure 18. While captured frames from camera-1 are directly passed on to the AU, the frames from camera-2 are filtered using AQuA, and sent to the AU (face detection) for processing. AU-specific estimator predicts the analytical quality, and the SARSA RL agent adjusts the camera parameters by using the VAPIX API provided by the camera vendor. We compared the accuracy of insights derived from the video feeds from camera-1 and camera-2. We observed an mAP improvement of 12% for Camera 2's video stream.

7 RELATED WORK

Several recent proposals have investigated the tuning of parameters of vision algorithms to improve computing resource usage of video analytics pipelines. VideoStorm [53] tunes parameters of vision algorithms like frames-per-second, frame resolution and internal algorithmic parameters (like the sliding window to search for objects in object detectors, for example) to ensure efficient resource management while processing video analytics queries. However, they do not address tuning of camera parameters. Similarly, Chameleon [21] dynamically picks the best configuration of values for algorithmic parameters like resolution, frame sampling rate, type of detector (e.g., Yolo, VGG or AlexNet) in typical neural-network based video analytics pipelines, based on the video content. However, they also do not address tuning of camera parameters to enhance video analytics.

Recent proposals have also considered optimizations to improve network resource usage of video analytics pipelines. AWStream [52] describes methods to make streaming applications to be adaptive by incorporating the ability to optimally trade-off accuracy of insights for wide-area network bandwidth consumption. Others [45] have considered sending the video stream in low resolution from

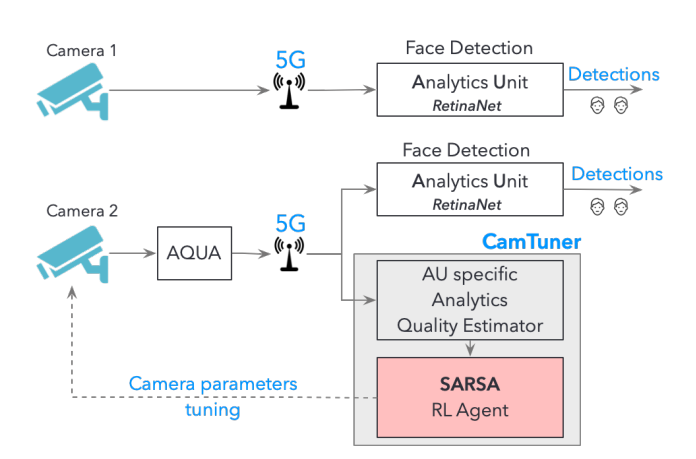


Figure 18: Deployment Setup

the edge to the cloud over a wide-area network, but recover the high-resolution frames from the low-resolution stream via a superresolution procedure tailored for the actual analytics tasks. A recent proposal [16] also suggests compressing regions of little or no interest more heavily while compressing regions of interest with a lower compression rate to better use the scarce network bandwidth between the sensor and the analytics server. Again, none of these approaches consider dynamic tuning of camera parameters to adapt to changing environmental conditions. Focus [19] uses a lightweight tiny-yolo model executing on the sensor device to screen frames that are sent for further analytics processing. Others [7, 22] propose binary classifiers to screen frames for analytics processing only when the frames contain the object of interest. The goal here is to reduce the network resource usage. Several techniques [8, 27] also compare consecutive frames and exploit temporal redundancy in video streams to screen frames that are considered for analytics processing. In our proposed approach, we use AQuA [33] to screen poor-quality frames to reduce network bandwidth usage. However, all these methods do not consider dynamic tuning of camera parameters to enhance the quality of the sensor output.

There is a considerable body of work to configure image signal processing pipeline (ISP) in cameras to improve human-perceived quality of images from the cameras. For example, VisionISP [50] modifies the ISP pipeline to reduce the size of final image output by reducing the bit-depth and resolution. Others have proposed custom optimizations of the ISP for specific computer-vision tasks [15, 18, 18, 28, 31, 39, 50, 54]. However, careful re-design or optimization of ISP module for specific vision tasks is time consuming. In our proposed approach, we do not modify the ISP pipeline, and focus on dynamic tuning of configurable camera parameters to consistently produce high-quality sensor output, and enhance the quality of insights from analytics tasks.

8 CONCLUSION

Complex sensors like video cameras have tens of configurable parameters that can be set by end-users to customize the sensors to specific application scenarios. These parameter settings have a significant impact on the quality of the sensor output, and the accuracy of insights derived from sensor data. However, most endusers use a fixed parameter setting because they lack the skill or understanding to appropriately configure these parameters. We proposed CamTuner, which is a system to automatically, and dynamically adapt the complex sensor to changing environmental conditions. Such dynamic tuning is done while the application has been deployed and is in service in the real world. We show that by automatically, and dynamically updating the parameter settings to adjust to changing environmental conditions near the sensor, our system can significantly improve the accuracy of inferred insights. Also, our proposed sensor modelling and dynamic tuning methodology can be used to automatically, and dynamically tune other complex sensors.

REFERENCES

- $[1] \ [n.d.]. \ Pillow \ Library. \ https://pillow.readthedocs.io/en/stable/.$
- [2] 2017. Vp9. https://www.webmproject.org/vp9/.
- [3] 2020. Smart sensor market type and size: 2027. https://www.marketsandmarkets.com/Market-Reports/smart-sensor-market-43119772.html
- [4] 2021. x264library. http://www.videolan.org/developers/x264.html.
- [5] Bryce E Bayer. 1976. Color imaging array. US Patent 3,971,065.
- [6] Vladimir Bychkovsky, Sylvain Paris, Eric Chan, and Frédo Durand. 2011. Learning Photographic Global Tonal Adjustment with a Database of Input / Output Image Pairs. In The Twenty-Fourth IEEE Conference on Computer Vision and Pattern Recognition.
- [7] Christopher Canel, Thomas Kim, Giulio Zhou, Conglong Li, Hyeontaek Lim, David G Andersen, Michael Kaminsky, and Subramanya Dulloor. 2019. Scaling Video Analytics on Constrained Edge Nodes. In Proceedings of Machine Learning and Systems, A. Talwalkar, V. Smith, and M. Zaharia (Eds.), Vol. 1. 406–417. https://proceedings.mlsys.org/paper/2019/file/85d8ce590ad8981ca2c8286f79f59954-Paper.pdf
- [8] Tiffany Yu-Han Chen, Lenin Ravindranath, Shuo Deng, Paramvir Bahl, and Hari Balakrishnan. 2015. Glimpse: Continuous, real-time object recognition on mobile devices. In Proceedings of the 13th ACM Conference on Embedded Networked Sensor Systems. 155–168.
- [9] CNET. 2019. How 5G aims to end network latency CNET_5G_network_latency_time.
- [10] cocoapi github. [n.d.]. pycocotools. https://github.com/cocodataset/cocoapi/tree/master/PythonAPI/pycocotools.
- [11] Axis Communications. [n.d.]. VAPIX Library. https://www.axis.com/vapixlibrary/
- [12] Eduardo Cuervo, Alec Wolman, Landon P. Cox, Kiron Lebeck, Ali Razeen, Madan Musuvathi, and Stefan Saroiu. 2015. Kahawai: High-Quality Mobile Gaming Using GPU Offload. In MobiSys'15. ACM – Association for Computing Machinery. https://www.microsoft.com/en-us/research/publication/kahawai-highquality-mobile-gaming-using-gpu-offload/
- [13] Jia Deng, Wei Dong, Richard Socher, Li-Jia Li, Kai Li, and Li Fei-Fei. 2009. Imagenet: A large-scale hierarchical image database. In 2009 IEEE conference on computer vision and pattern recognition. IEEE, 248–255.
- [14] Jiankang Deng, Jia Guo, Zhou Yuxiang, Jinke Yu, Irene Kotsia, and Stefanos Zafeiriou. 2019. RetinaFace: Single-stage Dense Face Localisation in the Wild. In arxiv.
- [15] Steven Diamond, Vincent Sitzmann, Frank Julca-Aguilar, Stephen Boyd, Gordon Wetzstein, and Felix Heide. 2021. Dirty Pixels: Towards End-to-end Image Processing and Perception. ACM Transactions on Graphics (TOG) 40, 3 (2021), 1–15.
- [16] Kuntai Du, Ahsan Pervaiz, Xin Yuan, Aakanksha Chowdhery, Qizheng Zhang, Henry Hoffmann, and Junchen Jiang. 2020. Server-Driven Video Streaming for Deep Learning Inference. In Proceedings of the Annual conference of the ACM Special Interest Group on Data Communication on the applications, technologies, architectures, and protocols for computer communication. 557–570.
- [17] Vikas Gaikwad and Rachita Rake. 2021. Video Analytics Market Statistics: 2027. https://www.alliedmarketresearch.com/video-analytics-market
- [18] Felix Heide, Markus Steinberger, Yun-Ta Tsai, Mushfiqur Rouf, Dawid Pajak, Dikpal Reddy, Orazio Gallo, Jing Liu, Wolfgang Heidrich, Karen Egiazarian, et al. 2014. Flexisp: A flexible camera image processing framework. ACM Transactions on Graphics (TOG) 33, 6 (2014), 1–13.
- [19] Kevin Hsieh, Ganesh Ananthanarayanan, Peter Bodik, Shivaram Venkataraman, Paramvir Bahl, Matthai Philipose, Phillip B. Gibbons, and Onur Mutlu. 2018. Focus: Querying Large Video Datasets with Low Latency and Low Cost. In 13th USENIX Symposium on Operating Systems Design and Implementation (OSDI 18). USENIX Association, Carlsbad, CA, 269–286. https://www.usenix.org/conference/osdi18/ presentation/hsieh
- [20] Si Young Jang, Yoonhyung Lee, Byoungheon Shin, and Dongman Lee. 2018. Application-aware IoT camera virtualization for video analytics edge computing. In 2018 IEEE/ACM Symposium on Edge Computing (SEC). IEEE, 132–144.
- [21] Junchen Jiang, Ganesh Ananthanarayanan, Peter Bodik, Siddhartha Sen, and Ion Stoica. 2018. Chameleon: scalable adaptation of video analytics. In Proceedings of the 2018 Conference of the ACM Special Interest Group on Data Communication. 253–266.
- [22] Daniel Kang, John Emmons, Firas Abuzaid, Peter Bailis, and Matei Zaharia. 2017. NoScope: Optimizing Neural Network Queries over Video at Scale. Proc. VLDB Endow. 10, 11 (Aug. 2017), 1586–1597. https://doi.org/10.14778/3137628.3137664
- [23] Vahid Kazemi and Josephine Sullivan. 2014. One millisecond face alignment with an ensemble of regression trees. In Proceedings of the IEEE conference on computer vision and pattern recognition. 1867–1874.
- [24] Diederik P Kingma and Jimmy Ba. 2014. Adam: A method for stochastic optimization. arXiv preprint arXiv:1412.6980 (2014).
- [25] Alex Krizhevsky, Ilya Sutskever, and Geoffrey E Hinton. 2012. Imagenet classification with deep convolutional neural networks. In Advances in neural information processing systems. 1097–1105.

- [26] H. Kuehne, H. Jhuang, E. Garrote, T. Poggio, and T. Serre. 2011. HMDB: a large video database for human motion recognition. In Proceedings of the International Conference on Computer Vision (ICCV).
- [27] Yuanqi Li, Arthi Padmanabhan, Pengzhan Zhao, Yufei Wang, Guoqing Harry Xu, and Ravi Netravali. 2020. Reducto: On-Camera Filtering for Resource-Efficient Real-Time Video Analytics. In Proceedings of the Annual conference of the ACM Special Interest Group on Data Communication on the applications, technologies, architectures, and protocols for computer communication. 359–376.
- [28] Lin Liu, Xu Jia, Jianzhuang Liu, and Qi Tian. 2020. Joint demosaicing and denoising with self guidance. In Proceedings of the IEEE/CVF Conference on Computer Vision and Pattern Recognition. 2240–2249.
- [29] Ziwei Liu, Ping Luo, Xiaogang Wang, and Xiaoou Tang. 2015. Deep Learning Face Attributes in the Wild. In Proceedings of International Conference on Computer Vision (ICCV).
- [30] Juan Carlos Niebles, Chih-Wei Chen, and Li Fei-Fei. 2010. Modeling temporal structure of decomposable motion segments for activity classification. In European conference on computer vision. Springer, 392–405.
- [31] Jun Nishimura, Timo Gerasimov, Sushma Rao, Aleksandar Sutic, Chyuan-Tyng Wu, and Gilad Michael. 2019. Automatic ISP image quality tuning using nonlinear optimization. arXiv:1902.09023 [cs.CV]
- [32] openvinotoolkit. [n.d.]. Computer Vision Annotation Tool (CVAT). https://github.com/openvinotoolkit/cvat.
- [33] Sibendu Paul, Utsav Drolia, Y. Charlie Hu, and Srimat T. Chakradhar. 2021. AQuA: Analytical Quality Assessment for Optimizing Video Analytics Systems. arXiv:2101.09752 [eess.IV]
- [34] Qualcomm. 2019. How 5G low latency improves your mobile experiences. Qualcomm_5G_low-latency_improves_mobile_experience.
- [35] Rajeev Ramanath, Wesley E Snyder, Youngjun Yoo, and Mark S Drew. 2005. Color image processing pipeline. IEEE Signal Processing Magazine 22, 1 (2005), 34–43.
- [36] Amy R. Reibman. 2018. STRATEGIES FOR QUALITY-AWARE VIDEO CON-TENT ANALYTICS. In 2018 IEEE Southwest Symposium on Image Analysis and Interpretation (SSIAI). 77–80. https://doi.org/10.1109/SSIAI.2018.8470354
- [37] Christos Sagonas, Epameinondas Antonakos, Georgios Tzimiropoulos, Stefanos Zafeiriou, and Maja Pantic. 2016. 300 faces in-the-wild challenge: Database and results. *Image and vision computing* 47 (2016), 3–18.
- [38] Florian Schroff, Dmitry Kalenichenko, and James Philbin. 2015. Facenet: A unified embedding for face recognition and clustering. In Proceedings of the IEEE conference on computer vision and pattern recognition. 815–823.
- [39] Eli Schwartz, Raja Giryes, and Alex M Bronstein. 2018. DeepISP: Toward learning an end-to-end image processing pipeline. IEEE Transactions on Image Processing 28, 2 (2018), 912–923.
- [40] Statisticssolutions. 2019. Pearson Correlation Coefficient. statistics-correlation-range.
- [41] Richard S Sutton, Andrew G Barto, et al. 1998. Introduction to reinforcement learning. Vol. 135. MIT press Cambridge.
- [42] Christian Szegedy, Vincent Vanhoucke, Sergey Ioffe, Jon Shlens, and Zbigniew Wojna. 2016. Rethinking the inception architecture for computer vision. In Proceedings of the IEEE conference on computer vision and pattern recognition. 2818–2826
- [43] Mingxing Tan, Ruoming Pang, and Quoc V Le. 2020. Efficientdet: Scalable and efficient object detection. In Proceedings of the IEEE/CVF conference on computer vision and pattern recognition. 10781–10790.
- [44] thebmj. 2019. correlation-and-regression. correlation-range.
- [45] Yiding Wang, Weiyan Wang, Junxue Zhang, Junchen Jiang, and Kai Chen. 2019. Bridging the Edge-Cloud Barrier for Real-time Advanced Vision Analytics. In 11th USENIX Workshop on Hot Topics in Cloud Computing (HotCloud 19). USENIX Association, Renton, WA. https://www.usenix.org/conference/hotcloud19/presentation/wang
- [46] Zhou Wang, A.C. Bovik, H.R. Sheikh, and E.P. Simoncelli. 2004. Image quality assessment: from error visibility to structural similarity. *IEEE Transactions on Image Processing* 13, 4 (2004), 600–612. https://doi.org/10.1109/TIP.2003.819861
- [47] Marco Wiering and Jürgen Schmidhuber. 1998. Fast Online Q(λ). Machine Learning 33, 1 (01 Oct 1998), 105–115. https://doi.org/10.1023/A:1007562800292
 [48] wikipedia. [n.d.]. L1 norm. https://en.wikipedia.org/wiki/Norm_(mathematics).
- [49] Wikipedia. [n.d.]. Precision and Recall. https://en.wikipedia.org/wiki/Precision_
- [50] Chyuan-Tyng Wu, Leo F Isikdogan, Sushma Rao, Bhavin Nayak, Timo Gerasimow, Aleksandar Sutic, Liron Ain-kedem, and Gilad Michael. 2019. VisionISP: Repurposing the image signal processor for computer vision applications. In 2019 IEEE International Conference on Image Processing (ICIP). IEEE, 4624–4628.
- [51] Lucie Yahiaoui, Jonathan Horgan, Brian Deegan, Senthil Yogamani, Ciarán Eising, and Patrick Denny. 2019. Overview and Empirical Analysis of ISP Parameter Tuning for Visual Perception in Autonomous Driving. *Journal of Imaging* 5 (09 2019), 78. https://doi.org/10.3390/jimaging5100078
- [52] Ben Zhang, Xin Jin, Sylvia Ratnasamy, John Wawrzynek, and Edward A Lee. 2018. Awstream: Adaptive wide-area streaming analytics. In Proceedings of the 2018 Conference of the ACM Special Interest Group on Data Communication. 236–252.

- [53] Haoyu Zhang, Ganesh Ananthanarayanan, Peter Bodik, Matthai Philipose, Paramvir Bahl, and Michael J. Freedman. 2017. Live Video Analytics at Scale with Approximation and Delay-Tolerance. In 14th USENIX Symposium on Networked Systems Design and Implementation (NSDI 17). USENIX Association, Boston, MA, 377–392. https://www.usenix.org/conference/nsdi17/technicalsessions/presentation/zhang
- [54] Kai Zhang, Wangmeng Zuo, and Lei Zhang. 2018. FFDNet: Toward a fast and flexible solution for CNN-based image denoising. IEEE Transactions on Image Processing 27, 9 (2018), 4608–4622.
- [55] Jianping Zhou and John Glotzbach. 2007. Image Pipeline Tuning for Digital Cameras. In 2007 IEEE International Symposium on Consumer Electronics. 1–4. https://doi.org/10.1109/ISCE.2007.4382143